UC Berkeley
UC Berkeley Previously Published Works

Title

Single-Molecule Imaging Reveals a Collapsed Conformational State for DNA-Bound Cohesin

Permalink

https://escholarship.org/uc/item/8900v68b

Journal

Cell Reports, 15(5)

ISSN

2639-1856

Authors

Stigler, Johannes
Çamdere, Gamze Ö
Koshland, Douglas E
et al.

Publication Date

2016-05-01

DOI

10.1016/j.celrep.2016.04.003

Peer reviewed

Single-molecule imaging reveals a collapsed conformational state for DNA-bound cohesin

Johannes Stigler[1], **Gamze Ö. Çamdere**[2], **Douglas E. Koshland**[2], and **Eric C. Greene**[1]

[1]Department of Biochemistry and Molecular Biophysics, Columbia University, New York, NY 10032

[2]Department of Molecular and Cell Biology, University of California, Berkeley, CA 94720

Abstract

Cohesin is essential for the hierarchical organization of the eukaryotic genome and plays key roles in many aspects of chromosome biology. The conformation of cohesin bound to DNA remains poorly defined, leaving crucial gaps in our understanding of how cohesin fulfills its biological functions. Here we use single molecule microscopy to directly observe the dynamic and functional characteristics of cohesin bound to DNA. We show that cohesin can undergo rapid one-dimensional (1D) diffusion along DNA, but individual nucleosomes, nucleosome arrays, and other protein obstacles significantly restrict its mobility. We further demonstrate that DNA motor proteins can readily push cohesin along DNA, but they cannot pass through the interior of the cohesin ring. Together, our results reveal that DNA-bound cohesin has a central pore that is substantially smaller than anticipated. These findings have direct implications for understanding how cohesin and other SMC proteins interact with and distribute along chromatin.

Introduction

Cohesin has important roles in the establishing the high-order organization of the eukaryotic genome, principally in coordinating the alignment and cohesion of sister chromatids prior to chromosome segregation, and is also crucial for regulating gene expression, DNA repair, and DNA replication (Dorsett and Ström, 2012; Dowen and Young, 2014; Michaelis et al., 1997; Mizuguchi et al., 2014; Sjögren and Nasmyth, 2001; Wendt et al., 2008). Defects in either cohesin or its regulatory factors can lead to chromosome nondisjunction and aneuploidy. Furthermore, mutations in human cohesin give rise to severe developmental disorders, such as Cornelia de Lange or Roberts syndrome (Horsfield et al., 2012; Krantz et al., 2004), and have also been implicated in myeloid leukemogenesis (Kon et al., 2013).

Cohesin consists of two members of the SMC (structural maintenance of chromosomes) family: Smc1 and Smc3 (Psm1 and Psm3 in *S. pombe*), which form anti-parallel coiled coils that dimerize at a central hinge. The terminal regions of Smc1 and Smc3 fold into nucleotide-binding head domains (Nasmyth, 2011; Nasmyth and Haering, 2009; Peters et al., 2008). The heads are bridged by Mcd1 (Rad21 in *S. pombe*), which is predicted to be largely unstructured, and contains binding sites for Scc3 and Pds5 (Chan et al., 2013; Roig et al., 2014), forming a tripartite ring-like complex (Gligoris et al., 2014) (Figure 1A).

Cohesin is enriched at centromeres and clusters along chromosome arms at ~10-kbp intervals at AT-rich cohesin associated regions (CARs) (Blat and Kleckner, 1999; Glynn et al., 2004; Laloraya et al., 2000). Cohesin is loaded by Scc2/4 (Mis4/Ssl3 in S. pombe), and is thought to spread into flanking genomic regions by 1D diffusion (Ocampo-Hafalla and Uhlmann, 2011). In both *S. cerevisiae* and *S. pombe*, cohesin is also enriched at sites of convergent transcription even though many of these sites lack the loader, suggesting that the transcriptional machinery may push cohesin to these locations (Glynn et al., 2004; Gullerova and Proudfoot, 2008; Lengronne et al., 2004). Thus, the *in vivo* distribution of cohesin is thought to arise from its interactions with the loader and from the ability of cohesin to move along chromatin.

Cohesin links sister chromatids from S-phase to the onset of chromosome segregation. The establishment of sister chromatid cohesion is generally thought of as a two-step process involving stable DNA binding by cohesin, often prior to S phase, followed by tethering of the two sister chromatids in S phase (Nasmyth, 2011). Electron microscopy (EM) studies reveal that cohesin can exist in its DNA-free form as a ring-like complex with a large central pore approximately 30–40-nm in diameter (Huis in 't Veld et al., 2014). It has been hypothesized that cohesin rings establish sister chromatid cohesion by topologically embracing the two DNA strands (Gligoris et al., 2014; Nasmyth, 2011; Nasmyth and Haering, 2009), and it has also been proposed that this establishment occurs by the passage of a replication fork through the ring (Lengronne et al., 2006). However, alternative models for cohesion invoke bridging interactions between different cohesin complexes bound to each of the two sister chromatids (Huang et al., 2005; Zhang et al., 2008). Interestingly, the ring-like structure reported for cohesin in the absence of DNA is distinct from the more rod-like conformations exhibited by many other SMC proteins (Soh et al., 2015). A major impediment to understanding cohesion, as well as the understanding of the many other biological roles of cohesin, has been the lack of evidence for the conformational state of DNA-bound cohesin and the overall poor understanding of how cohesin behaves while bound to DNA

The characteristics of cohesin bound to DNA remain poorly understood, cohesin-loader interactions have not been thoroughly characterized, and while there is evidence for topological binding (Gligoris et al., 2014; Ivanov and Nasmyth, 2005; Nasmyth and Haering, 2009; Ocampo-Hafalla and Uhlmann, 2011; Onn and Koshland, 2011), neither the size of the pore of the DNA-bound complex, nor the diffusive characteristics of cohesin are known. To address these issues, we sought to visualize the behavior of cohesin bound to individual molecules of DNA in real time. Our findings support a model in which cohesin is topologically bound to DNA, but exhibits characteristics most consistent with a small pore

diameter, suggesting a more rod-like binding configuration. These findings have direct implications for understanding how cohesin interacts with chromatin.

Results

Cohesin is targeted to A/T rich regions and CAR sequences

We purified tetrameric *S. pombe* cohesin (Psm1, Psm3, Psc3, Rad21; Figure 1A) and loader (Mis4/Ssl3) as described (Murayama and Uhlmann, 2014) and performed bulk biochemical experiments to ensure that these purified complexes reproduce previously identified properties. Purified cohesin showed basal ATP hydrolysis activity that was stimulated by Mis4/Ssl3, as expected (Murayama and Uhlmann, 2014), and also formed complexes resistant to washes of 500-mM KCl on DNA coupled to magnetic beads (Figure S1A,B), as previously reported *in vitro* (Murayama and Uhlmann, 2014; Onn and Koshland, 2011) and *in vivo* (Ciosk et al., 2000).

To visualize individual molecules of cohesin, we first incubated Mis4/Ssl3 and cohesin with λ-DNA (48.5-kb) in the presence of 0.5-mM ATP. The cohesin-bound DNA molecules were then anchored to a lipid bilayer deposited onto a flow-cell surface and aligned into single-tethered DNA curtains using nanofabricated barriers, as previously described (Figure 1B) (Greene et al., 2010). The DNA was stained with YOYO1 and visualized by total internal reflection fluorescence microscopy (TIRFM). Cohesin was labeled with quantum dots (QDs) targeted against the 3×V5 tag on Psm3 (Figure 1C). The correlated movement of labeled protein with the DNA upon changes in flow rate allowed us to confirm that all identified proteins were bound to DNA and not adsorbed to the flowcell surface. The loading efficiency was dependent on the concentration of monovalent salt, requiring at least 10-mM KCl, but was inhibited at concentrations exceeding 80-mM KCl, suggesting that electrostatic interactions may play a role in the recruitment of cohesin to DNA.

These experiments revealed that cohesin preferentially localizes to one half of the λ-DNA (Figure 1D). The localization positions are highly correlated (Pearson's r=0.90) with A/T nucleotide content (Figure 1D), consistent with the behavior of cohesin *in vivo* (Blat and Kleckner, 1999; Glynn et al., 2004; Laloraya et al., 2000). We also determined the binding distribution of cohesin on λ-DNA containing a native 3-kb CAR sequence (λ^CAR) insert that was shown to be cohesin-enriched *in vivo* (Laloraya et al., 2000). Remarkably, cohesin also preferentially localized to the CAR insert, suggesting that the observed *in vitro* binding distribution reflected the physiological behavior of cohesin and its preference for A/T rich sites (Figure 1E), independently of DNA orientation (Figure S2A).

Cohesin is highly stable under a wide range of salt conditions

Experiments on double-tethered DNA curtains, where the free end of the λ^CAR-DNA molecule was anchored to chromium pedestals (Gorman et al., 2010; Greene et al., 2010), allowed us to observe DNA bound cohesin in the absence of buffer flow (Figure 2A). After assembly, free and weakly bound proteins were flushed from the sample chamber. As in the single-tethered case, cohesin preferentially bound to A/T-rich regions of the DNA (Figure 2B). To test the stability of these complexes under a wide range of buffer conditions, we then

exchanged the sample buffer with buffer (±0.5-mM ATP) at various concentrations of KCl, stopped the flow, and measured the lifetimes of DNA-bound complexes. The survival probabilities of cohesin after buffer exchange followed single exponential distributions, indicating that the molecules dissociate from the DNA through a single mechanism (Figure 2C). While the addition of ATP had little or no impact on the number of binding events in single molecule experiments or in bulk (Figure S1C,D), the presence of ATP yielded a ~1.5-fold increase in the cohesin lifetime relative to experiments without ATP (Figure 2D). In addition, stable cohesin remained tightly bound to the DNA even at the highest KCl concentration tested, exhibiting a lifetime of 13±3 minutes at 500-mM KCl (Figure 2C,D). Thus cohesin binding to DNA curtains reproduces the characteristics of cohesin-DNA complexes assembled either *in vitro* and *in vivo* (Ivanov and Nasmyth, 2005; Murayama and Uhlmann, 2014; Onn and Koshland, 2011).

Mis4/Ssl3 increases the transient lifetime of cohesin on DNA

To further assess the relevance of the observed cohesin-DNA complexes, we analyzed the impact of the loader on their assembly. We injected QD-tagged cohesin into a flow cell with a pre-assembled DNA curtain in the presence or absence of Mis4/Ssl3 and stopped the flow. We then measured the positions where cohesin bound to DNA and the lifetime of these interactions. While some cohesin binding was observed when Mis4/Ssl3 was absent, in the presence of Mis4/Ssl3 the number of cohesin binding events was dramatically increased (Figure 2E). These findings are similar to results reported previously for the assembly of cohesin with DNA in solution (Murayama and Uhlmann, 2014), suggesting that cohesin has an intrinsic ability to bind DNA and that this activity is enhanced by Mis4/Ssl3. The initial binding positions showed a strong preference for A/T-rich regions, suggesting that the observed A/T preference in equilibrated *in vitro* experiments (Figure 1) and *in vivo* (Blat and Kleckner, 1999; Glynn et al., 2004; Laloraya et al., 2000) is not a result of cohesin molecules that become loaded elsewhere and then transported, be it actively or passively, to A/T-rich regions. Instead, cohesin preferentially associates with DNA directly at the A/T-rich sites.

To characterize the stability of each sub-population, we determined their lifetimes. Without loader, we identified two classes of interactions: highly stable complexes (as described above) that persisted throughout the observation (τ 10-min), and transient complexes that exhibited a lifetime of just 32±7 seconds (Figure 2F). With loader present, we also observed a third class with an extended transient lifetime of 5±1 minutes (Figure 2F), indicating that this longer-lasting interaction is a signature of a Mis4/Ssl3-mediated loading intermediate. Interestingly, even though Mis4/Ssl3 can stimulate the ATP hydrolysis rate of cohesin (Murayama and Uhlmann, 2014), the lifetimes of the loading intermediates identified were did not require ATP (Figure 2F), suggesting that ATP hydrolysis does not contribute at this stage of loading.

Individual cohesin complexes diffuse on DNA

Many properties of cohesin are attributed to its ability to diffuse on DNA (Ocampo-Hafalla and Uhlmann, 2011), but the diffusive characteristics of cohesin remain unknown. DNA curtains offer the ability to measure the diffusive properties of cohesin through direct

observation. When visualized at low monovalent ionic strength (0-mM KCl), cohesin diffused slowly along the DNA and displayed a preference for localizing to A/T-rich regions (Figure 1C, 2B). When the ionic strength was increased, a varying fraction (~50–90%) quickly dissociated, while the remaining proteins began diffusing rapidly along the DNA (Figures 3A, S3A). The observed diffusion coefficients increased with increasing ionic strength (Figure 3B) but were independent of ATP (Figure S3B), in agreement with recent findings on the bacterial SMC complex BsSMC (Kim and Loparo, 2016). The theoretical upper limit for the diffusion of QD-tagged cohesin is determined by the diameter of the QD (~19.5-nm; Figure S3C,D), corresponding to a diffusion coefficient of ~23-μm^2/sec (assuming that cohesin does not track the helical trajectory of the phosphate backbone). Intriguingly, the diffusion coefficient for QD-tagged cohesin at 500-mM KCl was 3.8±0.2-μm^2/sec, which approaches the theoretical limit for free diffusion and is significantly larger than the upper limit for rotational diffusion along the backbone of ~0.03-μm^2/s (Bagchi et al., 2008; Blainey et al., 2009), suggesting that cohesin makes only weak contact with the DNA. Remarkably, the lifetime of cohesin is still ~10 minutes under these conditions, consistent with expectations for a topologically closed ring.

The strong A/T-binding preference of cohesin raises the question of whether cohesin might also diffuse differently on A/T-rich versus G/C-rich regions of DNA. Indeed, at low ionic strength cohesin displayed significantly slower diffusion in A/T-rich regions relative to G/C-rich regions (Figure 3C), but the sequence-dependent differences vanished at 500-mM KCl (Figure 3D). This sequence-dependent diffusion is likely a consequence of salt-dependent interactions between cohesin and DNA and together with the A/T-binding preference of Mis4/Ssl3, may explain why cohesin accumulates at A/T-rich regions of the genome (Blat and Kleckner, 1999; Glynn et al., 2004; Laloraya et al., 2000).

Cohesin is topologically loaded on DNA

Models invoking a topological binding mechanism in which cohesin encircles DNA predict, firstly, that the dissociation of freely diffusing cohesin complexes should occur preferentially from free DNA ends, and, secondly, that dissociation should not occur when these ends are blocked. We tested the first prediction using single-tethered DNA curtains (Figure 3E,F). Cohesin was initially loaded onto λ^{CAR} DNA at 30-mM KCl, and then chased with buffer containing 250-mM KCl. As expected, the binding distribution of cohesin at low salt was dictated by A/T content (Figure 3F). Upon switching the buffer to high salt, some cohesin dissociated directly into solution, without moving along the DNA. However, flow-induced hydrodynamic force pushed the remaining complexes rapidly along the DNA. Figure 3F shows dissociation position histograms for all tracked complexes, including the rapidly dissociating fraction (orange) and the subset of complexes that were pushed along DNA (red). These data indicate that cohesin dissociates from free DNA ends, as expected from sliding of a topologically closed ring.

We next used double-tethered curtains to determine whether blocking the DNA ends prevented dissociation. Cohesin was loaded onto double-tethered DNA at low ionic strength, and the sample chamber was flushed with buffer containing 500-mM KCl. In the absence of flow cohesin diffused rapidly along the DNA (Figure 3G). However, iterative pulses of

buffer flow pushed cohesin to the anchored DNA ends, but did not cause cohesin to dissociate into solution. Instead, cohesin resumed diffusing along the DNA as soon as buffer flow was stopped (Figure 3G). These results, along with the finding that cohesin remains bound to DNA for extended periods of time at high ionic strength, even though its rapid diffusion suggests it interacts only weakly with DNA, suggest that diffusive cohesin complexes are topologically bound to DNA.

We also used our characterization of cohesin's diffusion on DNA to estimate the salt-screenable electrostatic interaction energy with DNA (Slutsky and Mirny, 2004) (Supplemental methods and Figure S3E). This interaction energy by itself is insufficient to keep cohesin bound to DNA for more than a few milliseconds. The experimentally determined long lifetime of cohesin on DNA therefore argues for an additional energy contribution that keeps cohesin bound. Our analysis shows that this energy is much higher than the electrostatic interaction energy and independent of salt concentration, as expected from a topological interaction (Figure S3F).

CAR sites do not cause a different mode of cohesin binding

The previously described single tethered sliding assay allowed us to test if cohesins that are loaded at native CAR sites are likelier to slide on DNA, that is, likelier be topologically loaded, than cohesins loaded elsewhere. Such a result could be expected if the sequence context of CAR sites causes enhanced topological loading. However, the tracking of cohesin that dissociated from the free DNA end revealed that their initial binding position was solely predicated by A/T content, and complexes loaded at the CARS behaved similarly to those loaded elsewhere on the DNA (Figure S2B). We conclude that cohesin loaded at CAR sites are biochemically indistinguishable from cohesin loaded elsewhere on the DNA.

Mis4/Ssl3 diffuses on DNA

The DNA curtain assay also allowed us to test the DNA binding properties of the loader complex Mis4/Ssl3. We began by assessing the binding of QD-tagged Mis4/Ssl3 in the absence of cohesin. Mis4/Ssl3 bound to and diffused slowly along the DNA, exhibiting a lifetime of 20 ± 2 minutes and a 1D diffusion coefficient of 0.016 ± 0.003-μm^2/sec (Figure S4A,B). Mis4/Ssl3 also preferentially bound A/T-rich regions (Figure S4C), but most of the protein (85–97%) dissociated when chased with 500-mM KCl (Figure S4D). The finding that Mis4/Ssl3 shows a preference for A/T-rich DNA and can also undergo 1D diffusion suggests the possibility that some cohesin may remain associated with the loader while bound to DNA. Indeed, cohesin and loader often colocalize on chromatin (Kogut et al., 2009; Lengronne et al., 2004), and a small fraction of Mis4/Ssl3 resists dissociation from DNA at 500-mM KCl in our bulk and single molecule assays (Figure S1G & Figure S4). However, the diffusive properties and localization of cohesin in the absence or presence of loader were identical, suggesting that cohesin was not indirectly bound to DNA through its association with Mis4/Ssl3. Consistent with this conclusion, we were unable to detect persistent co-localization of cohesin and Mis4/Ssl3 on the DNA.

Collision experiments reveal a small pore size

Popular models suggest that cohesin exists as a ring-like structure with a large central pore that is big enough to incorporate two chromatin fibers (Haarhuis et al., 2014; Nasmyth and Haering, 2009). To measure the functional diameter of the pore we asked whether cohesin could diffuse past obstacles of varying diameters located at defined positions on the DNA (Figure 4A). We first tested whether cohesin is capable of diffusing past digoxigenin (dia. ~1–2-nm) that was covalently linked to the DNA (see supplemental methods). These experiments revealed that cohesin could diffuse freely past digoxigenin (Figure 4B). In striking contrast, digoxigenin that was labeled with a QD (dia. ~19.5-nm) acted as an impenetrable barrier to cohesin diffusion (Figure 4B). This result indicates that the pore size is smaller than the ~30–40-nm diameter implied by EM-studies (Huis in 't Veld et al., 2014).

We next tested whether cohesin is capable of diffusing past DNA-bound proteins of intermediate diameters, including catalytically inactive versions of EcoRI (EcoRI^{E111Q}; dia. ~6.4-nm) and dCas9 (dia. ~10.6-nm) (Figure S5). Cohesin could diffuse past unlabeled EcoRI^{E111Q} and dCas9, but was unable to bypass QD-tagged dCas9 (Figure 4C,D). Inspection of the diffusion trajectories revealed evidence of semi-permeable barriers that hindered the diffusion of cohesin at positions coincident with the binding sites for unlabeled EcoRI^{E111Q} and dCas9 (Figure 4C,D & Figure S6A,B), revealing the locations of these proteins even though they were not fluorescently labeled. To more precisely define the sites of hindered diffusion we calculated the permeability index profile μ(x) for individual diffusion trajectories at each position on the DNA (see supplemental methods). A freely diffusing molecule will yield a permeability index of μ=1, whereas obstacles that hinder diffusion will be revealed as dips in the permeability index (Figure S7A). Permeability index profiles of naked DNA showed no evidence for hindered diffusion (Figure 4E). In contrast, cohesin diffusion on DNA bound by either EcoRI^{E111Q} or dCas9 revealed semi-permeable diffusion barriers at the binding sites for EcoRI^{E111Q} or dCas9 (Figure 4E, S6E). Our results show that cohesin is able to bypass a barrier of ~10.6-nm in diameter but is unable to overcome a ~19.5-nm obstacle. We conclude that DNA-bound proteins can significantly hinder the diffusion of cohesin relative to its behavior on naked DNA.

Cohesin can be pushed by DNA motor proteins

Cohesin is abundant at sites of convergent transcription in yeast and it has been suggested that RNA polymerase may push cohesin to these locations (Glynn et al., 2004; Gullerova and Proudfoot, 2008; Lengronne et al., 2004; Ocampo-Hafalla and Uhlmann, 2011). As a direct test of the plausibility of this model we sought to determine whether a DNA motor protein is capable of pushing cohesin. As a proxy for the transcriptional machinery we chose FtsK (dia. ~12.6-nm), which is a highly processive translocase capable of dislodging other proteins from DNA (Lee et al., 2014; Marquis et al., 2008) (Figure 5A). We asked whether FtsK could push cohesin at low ionic strength, where cohesin exhibits the least mobility, ensuring that we could distinguish FtsK-induced movement from the translocase-independent diffusion of cohesion observed at higher ionic strength. Remarkably, FtsK could push cohesin for several kilobases (Figure 5B), even though cohesin alone exhibits relatively little mobility under these conditions. FtsK moves on DNA in a characteristic zig-zag pattern and randomly changes direction (Lee et al., 2014). Importantly, cohesin was left behind at

the sites where FtsK changed direction, confirming that the motor-induced movement of cohesin was due to a pushing force and that cohesin remained bound to the DNA while being pushed by the translocase (Figure 5B). We conclude that cohesin is readily pushed by a model DNA translocase. The inability of FtsK to bypass cohesin suggests that DNA motor proteins with diameters exceeding ~13-nm would not be able to pass through the cohesin ring.

Chromatin restricts the movement of cohesin

Nucleosomes are likely the most common DNA-bound obstacle encountered by cohesin *in vivo*. Therefore, we next asked whether cohesin is capable of diffusing past individual nucleosomes (Figure 5C). Interestingly, cohesin was able to diffuse past unlabeled nucleosomes (Figure 5D, S6C), but similar to what was observed for EcoRI^{E111Q} and dCas9, the individual nucleosomes acted as semi-penetrable barriers that hindered diffusion (Figure 5E). The finding that a single nucleosome could hinder cohesin diffusion suggested that additional nucleosomes might have an even more pronounced effect. Indeed, the diffusion of cohesin was greatly restricted by higher density nucleosome arrays (Figure 5F), strongly suggesting that chromatin will substantially reduce cohesin movement along DNA *in vivo*.

Having observed that the diffusion of cohesin across single protein obstacles is hindered, we next sought to establish the effect of DNA covered with many protein obstacles on the diffusivity of cohesin. The highly restricted movement of cohesin observed on nucleosome arrays made it difficult to more quantitatively address how the diffusivity of cohesin was impacted on these crowded substrates. Instead, we quantified the extent to which a single protein obstacle hindered the diffusion of cohesin and then used this information to more precisely predict how more crowded settings would impact the movement of cohesin along DNA. The frequency of obstacle crossings is directly related to an obstacle's microscopic permeability κ (Novikov et al., 2011), a quantity closely related to the permeability index μ (see supplemental methods). This can be intuitively understood by considering that highly permeable obstacles will more frequently crossed than less permeable or impermeable obstacles. Therefore we recorded diffusion trajectories of cohesin on DNA bound by single protein roadblocks to extract the time that cohesin spends freely diffusing until it crosses an individual roadblock (Figure 6A,B). Using a maximum likelihood procedure, we validated that in the absence of roadblocks, cohesin showed unhindered diffusion (Figure S7B), and established an upper limit for the microscopic permeability of quantum dots (Figure S7C). We then determined the microscopic permeabilities for individual molecules of dCas9, EcoRI^{E111Q} and nucleosomes (Figure 6C–E). All three obstacles yielded similar permeabilities (Figure 6C–E), which allowed us to determine the effective reduction of the diffusion coefficient for cohesin on highly crowded substrates bearing randomly distributed protein obstacles separated from one another by a defined average distance (Figure 6F) and verify the effect of reduced diffusion qualitatively in simulations (Figure S7D). The average length of the linker DNA between adjacent nucleosomes in *S. pombe* is ~20-bp (Moyle-Heyrman et al., 2013), which would yield a ~3000-fold reduction in the diffusivity of cohesin relative to its movement on naked DNA (Figure 6F). This finding highlights the impact that crowded physiological settings are anticipated to have on the diffusive motion of

cohesin bound to DNA. Interestingly, while the observed hindrance likely prevents diffusive spreading over whole chromosomes, it would still allow cohesin to travel over intermediate distances on biologically relevant timescales. We estimate that within one hour, cohesin may still spread by diffusion over distances of up to 7-kb on chromatin.

Discussion

Here we have established a single-molecule microscopy assay to directly visualize and characterize single cohesin complexes bound to DNA. Our experiments recapitulate many physiological characteristics of cohesin and also provide crucial insights into how cohesin interacts with DNA and chromatin.

Factors influencing the distribution of cohesin

Cohesin is not homogeneously distributed along chromosome arms, but instead is located primarily in A/T-rich regions (Blat and Kleckner, 1999; Glynn et al., 2004; Laloraya et al., 2000). The mechanisms contributing to these observed *in vivo* distributions remain poorly understood. Importantly, our results recapitulate the physiological preference of cohesin for A/T-rich DNA, and we find that cohesin interacts directly or indirectly with A/T-rich regions in multiple ways. First, cohesin directly binds to DNA from solution at A/T-rich sequences. Second, the Mis4/Ssl3 loader also showed preference for A/T-rich sequences and enhanced the loading of cohesin at these sites. Third, the diffusion of cohesin on DNA is correlated with A/T content at low ionic strength and its diffusion is slowed on A/T-rich sequences. We propose that the combination of these three interaction mechanisms contribute to the accumulation of cohesin in A/T-rich regions on chromosomes.

ChIP data has also revealed that some cohesin peaks *in vivo* did not superimpose with loader peaks (Kogut et al., 2009; Lengronne et al., 2004), suggesting that cohesin may move away from sites where they were loaded. Cohesin was often found at sites of convergent transcription (Glynn et al., 2004; Lengronne et al., 2004), suggesting that transcribing RNA polymerases might be pushing cohesin along chromatin. Our experiments demonstrate that cohesin can be pushed by a motor protein comparable in size to RNA polymerase, suggesting that transcription-induced mobility is feasible scenario for the localization of cohesin at sites of convergent genes. In addition, we show that free diffusion of cohesin along on chromatin is highly restricted, supporting the notion that the removal of histones from actively transcribed genes may facilitate re-localization of cohesin towards regions of convergent transcription. Interestingly, it has been recently found that the maintenance of nucleosome-free regions in yeast is also mediated by the loader (Lopez-Serra et al., 2014), suggesting that the loader may facilitate dispersal of cohesin away from the sites where it is initially loaded.

Mechanism of DNA loading

The loading of cohesin *in vivo* is dependent on the loader (Ciosk et al., 2000), and experiments done *in vitro* have shown that the loader can substantially increase the amount of cohesin bound to DNA (Murayama and Uhlmann, 2014). Here we confirm this finding in a bead-based pulldown assay and in single molecule experiments, and we further

demonstrate that Mis4/Ssl3 facilitates the loading of free cohesin onto DNA by extending the time cohesin remains bound to DNA before it can convert to a topologically bound conformation (Figure 7A). Our data suggest that individual cohesin complexes can transiently bind to DNA for short times (τ ~30-s), but only a fraction of these interactions convert into a stable topologically loaded form before dissociation. Mis4/Ssl3 enhances the number of binding events and also gives rise to a new loading intermediate with a longer lifetime (τ ~5-min), thereby promoting the probability of forming topologically bound complexes (τ 10-min) by increasing the overall time that cohesin is associated with the DNA (Figure 7A). Future work will be necessary to determine whether the emergence of the second long-lived population stems from cohesin that interacts with DNA-bound Mis4/Ssl3 or from cohesin-Mis4/Ssl3 complexes that form in solution before interacting with DNA.

Interestingly, ATP had no influence on the lifetime of the observed binding events, suggesting that ATP binding or hydrolysis is not involved in the initial recruitment of cohesin or the Mis4/Ssl3-mediated loading intermediate. FRAP studies in HeLa cells have also identified short and long-lived interactions of cohesin with chromatin, with remarkably similar lifetimes to those found in this study (Ladurner et al., 2014), suggesting that the dynamic binding mode identified in FRAP experiments (Gerlich et al., 2006; Ladurner et al., 2014) and the Mis4/Ssl3-dependent loading intermediate identified here may be the same.

Cohesin binds DNA in a compact conformational state

There is no detailed structural information available for cohesin bound to DNA. However, electron microscopy has provided coarse structural information for free cohesin, showing that in the absence of DNA a sizeable proportion of molecules adopt a large ring-like conformation (Anderson et al., 2002; Huis in 't Veld et al., 2014). The stability of cohesin-DNA interactions at high ionic strength (Ciosk et al., 2000) and experiments where the interfaces of the tripartite ring have been crosslinked (Gligoris et al., 2014; Haering et al., 2008), suggest a topological binding model where cohesin wraps around the DNA. Our experiments corroborate this finding and show that single cohesin complexes are topologically bound to bare DNA. However, the inability of cohesin to bypass ~20-nm sized quantum dots and its hindered diffusion when bypassing smaller obstacles challenge the idea that cohesin is bound to DNA in a large-ring conformation. Instead, our data suggest that the size of the pore is smaller than the ~30–40-nm suggested by EM images in the absence of DNA. Our data are most consistent with DNA binding in a more constrained rod-like ring conformation (Figure 7B). Topological binding and a rod-like conformation do not contradict each other as evidenced by condensin, a close relative of cohesin that exhibits both properties (Barysz et al., 2015). Moreover, crosslinking experiments have revealed that in the absence of DNA the coiled coils of the cohesin SMC proteins, which form the perimeter of the ring, come close to one another, either permanently or transiently, for long enough periods of time to be chemically crosslinked (Huis in 't Veld et al., 2014). This finding directly implies that rod-like conformations must exist at least metastably, even in the absence of DNA. Interestingly, rod-like conformations seem to be the prevalent form observed for condensin and several other SMC complexes (Barysz et al., 2015; Soh et al., 2015). In addition, the MRN (Mre11/Rad50/Nbs1) complex undergoes a large conformational change a from ring-like structure in solution to a rod-like structure when it is

bound to DNA (Moreno-Herrero et al., 2005). Our data support the hypothesis that cohesin undergoes a similar conformational transition into a more rod-like architecture upon binding to DNA.

An alternative possibility is that the DNA may be bound in a location outside of the coiled coil region, and remains topologically trapped between the SMC heads and Rad21 (Figure 7B). Support for this alternative possibility stems from structural studies which suggest that in the SMC-like MRN complex, the DNA-binding site on Rad50 is within the globular head domains but outside of the central pore formed by the Rad50 coiled-coiled domains (Williams et al., 2008). Similarly, also in Smc5/6, the DNA binds to a sub-complex interacting with the head domains, outside of the coiled-coil pore (Zabrady et al., 2016). Future work mapping the precise path of DNA through cohesin will be necessary to test this alternative model.

Implications for sister chromatid cohesion

The topological embrace model where two DNA strands are captured topologically within central pore of cohesin has become popular. However, one important complication of this model is that it requires the cohesin ring to undergo multiple open and closing events. The first opening event would need to occur during initial loading of cohesin onto the DNA prior to S-phase, and the second event would be necessary to allow entry of the second DNA strand during S-phase. It remains unclear how this model would ensure that the first DNA does not simply escape when the second DNA is captured by the ring, and it also remains unclear what might prevent three or more DNA strands from entering the ring. One possible explanation is that the replisome might pass through the large pore of previously loaded cohesin (Figure 7C), which would preclude any requirement for a second ring opening event, and would also help coordinate the establishment of cohesion with the local passage of a replication fork (Lengronne et al., 2006). However, we have demonstrated that cohesin is easily pushed along DNA by the motor protein FtsK, which is only ~13-nm in diameter, but FtsK itself does not appear to be capable of passing through the cohesin pore. This finding strongly suggests that it would not be possible for the entire replisome to fit through the ring interior without invoking a replication-coupled mechanism for ring opening or other large structural reorganization. Nevertheless, if the replication fork cannot pass through the cohesin ring, a second ring opening event and repositioning of cohesin behind the fork would be required to prevent stalling replication when forks converge. Such repositioning has also been proposed for nucleosomes (Annunziato, 2005) and in the case of cohesin, would be expected to concur with acetylation of Smc3 by a fork-associated acetylase (Song et al., 2012).

Alternative models, such as the handcuff and bracelet models, have also been proposed for chromosome cohesin involving DNA strands that are bridged by multiple molecules of cohesin (Huang et al., 2005; Nasmyth, 2011). These models are all consistent with cohesin adopting a more rod-like structure (Figure 7D). An additional attraction of these models is that they invoke the formation of higher order cohesin structures, in which each individual cohesin is bound to just one DNA molecule, which eliminates any need for a second DNA loading event. Instead, cohesion is established through protein-protein interactions between

cohesin complexes that are bound to two different DNA molecules (Eng et al., 2015). Interestingly, remarkably similar models have also been reported for MRN, and the rod-like architecture of MRN allows it to bridge broken DNA molecules so that they can be more easily repaired by non-homologous end joining (NHEJ) (Moreno-Herrero et al., 2005). Indeed, AFM studies have directly revealed the existence of DNA molecules bridged by rod-like MRN complexes in a conformation akin the handcuff model for cohesin (Moreno-Herrero et al., 2005). Future studies will be necessary to determine if cohesin is capable of forming similar DNA-bridging interactions.

Conclusion

The results reported here directly visualize the interactions of single cohesin complexes with DNA. We were able to observe the topological loading of cohesin onto A/T rich DNA, and we were able to directly visualize and quantify the diffusive characteristics of cohesin on both naked DNA and DNA bound by protein obstacles. Our results reveal that the functional pore size of cohesin in its DNA-bound conformation is larger than ~10.6-nm but less than ~19.5-nm. A crucial implication of these findings is that the smaller-than-anticipated pore size for cohesin will greatly constrain its effective diffusivity and limits the potential for diffusive spreading by orders of magnitude in a physiologically crowded setting relative to naked DNA. Importantly, our findings of restricted diffusion across obstacles are inconsistent with prevalent models that suggest cohesin binds DNA in a large ring conformation and instead agree with a model in which cohesin adopts a more collapsed, perhaps rod-like, conformation when it is bound to DNA.

Methods

Cohesin and Mis4/Ssl3 loader were expressed and purified as described (Murayama and Uhlmann, 2014). Complexes were characterized in DNA binding and ATPase assays as described (Murayama and Uhlmann, 2014; Onn and Koshland, 2011). For single molecule experiments, proteins were labeled with quantum dots conjugated to antibodies against epitope tags. Single molecule cohesin experiments were conducted in a buffer containing 40-mM Tris-HCl pH 7.5, 30-mM KCl, 25-mM NaCl, 1-mM $MgCl_2$, 1-mM DTT, 1-mg/ml BSA, at 32°C. In experiments requiring the visualization of DNA, the sample buffer was supplemented with $0.2\times$ glucose oxidase/catalase, 0.8% glucose and 0.15-nM YOYO-1. Flow cells were constructed by nano-fabricating chromium barriers on a glass slide and assembled into flow chambers using double sided tape (Greene et al., 2010). DNA substrates were cloned, propagated in bacteriophage λ, generated in large quantity by lytic growth, purified and end-tagged with biotinylated or digoxigenylated oligos. DNA molecules were anchored to the surface using biotin-streptavidin interactions on a surface-deposited lipid bilayer. For experiments in the absence of flow, the free DNA ends were anchored to chromium pedestals about 12-μm downstream of the barriers using digoxigenin-antibody interactions. Microscopy was performed on a prism-type TIRF microscope equipped with a 488-nm laser and a microfluidics system that allowed the injection of sample and rapid exchange of buffers. Videos were recorded at 60, 100, 200 or 500-msec temporal resolution and analyzed using custom software in Igor Pro. Detailed methods are available in the Supplemental Information.

Supplementary Material

Refer to Web version on PubMed Central for supplementary material.

References

Anderson DE, Losada A, Erickson HP, Hirano T. Condensin and cohesin display different arm conformations with characteristic hinge angles. J Cell Biol. 2002; 156:419–424. [PubMed: 11815634]

Annunziato AT. Split decision: what happens to nucleosomes during DNA replication? J Biol Chem. 2005; 280:12065–12068. [PubMed: 15664979]

Bagchi B, Blainey PC, Xie XS. Diffusion constant of a nonspecifically bound protein undergoing curvilinear motion along DNA. J. Phys. Chem. B. 2008; 112:6282–6284. [PubMed: 18321088]

Barysz H, Kim JH, Chen ZA, Hudson DF, Rappsilber J, Gerloff DL, Earnshaw WC. Three-dimensional topology of the SMC2/SMC4 subcomplex from chicken condensin I revealed by cross-linking and molecular modelling. Open Biology. 2015; 5:150005–150005. [PubMed: 25716199]

Blainey PC, Luo G, Kou SC, Mangel WF, Verdine GL, Bagchi B, Xie XS. Nonspecifically bound proteins spin while diffusing along DNA. Nat Struct Mol Biol. 2009; 16:1224–1229. [PubMed: 19898474]

Blat Y, Kleckner N. Cohesins bind to preferential sites along yeast chromosome III, with differential regulation along arms versus the centric region. Cell. 1999; 98:249–259. [PubMed: 10428036]

Chan K-L, Gligoris T, Upcher W, Kato Y, Shirahige K, Nasmyth K, Beckouët F. Pds5 promotes and protects cohesin acetylation. PNAS. 2013; 110:13020–13025. [PubMed: 23878248]

Ciosk R, Shirayama M, Shevchenko A, Tanaka T, Toth A, Nasmyth K. Cohesin's binding to chromosomes depends on a separate complex consisting of Scc2 and Scc4 proteins. Mol. Cell. 2000; 5:243–254. [PubMed: 10882066]

Dorsett D, Ström L. The ancient and evolving roles of cohesin in gene expression and DNA repair. Curr. Biol. 2012; 22:R240–R250. [PubMed: 22497943]

Dowen JM, Young RA. SMC complexes link gene expression and genome architecture. Curr. Opin. Genet. Dev. 2014; 25:131–137. [PubMed: 24794701]

Eng T, Guacci V, Koshland D. Interallelic complementation provides functional evidence for cohesin-cohesin interactions on DNA. Mol Biol Cell. 2015; 26:4224–4235. [PubMed: 26378250]

Gerlich D, Koch B, Dupeux F, Peters J-M, Ellenberg J. Live-cell imaging reveals a stable cohesin-chromatin interaction after but not before DNA replication. Curr. Biol. 2006; 16:1571–1578. [PubMed: 16890534]

Gligoris TG, Scheinost JC, Burmann F, Petela N, Chan KL, Uluocak P, Beckouet F, Gruber S, Nasmyth K, Lowe J. Closing the cohesin ring: Structure and function of its Smc3-kleisin interface. Science. 2014; 346:963–967. [PubMed: 25414305]

Glynn EF, Megee PC, Yu H-G, Mistrot C, Unal E, Koshland DE, DeRisi JL, Gerton JL. Genome-wide mapping of the cohesin complex in the yeast Saccharomyces cerevisiae. PLoS Biol. 2004; 2:E259. [PubMed: 15309048]

Gorman J, Plys AJ, Visnapuu M-L, Alani E, Greene EC. Visualizing one-dimensional diffusion of eukaryotic DNA repair factors along a chromatin lattice. Nat Struct Mol Biol. 2010; 17:932–938. [PubMed: 20657586]

Author Manuscript Author Manuscript Author Manuscript Author Manuscript

Greene EC, Wind S, Fazio T, Gorman J, Visnapuu M-L. DNA curtains for high-throughput single-molecule optical imaging. Meth. Enzymol. 2010; 472:293–315. [PubMed: 20580969]

Gullerova M, Proudfoot NJ. Cohesin complex promotes transcriptional termination between convergent genes in S. pombe. Cell. 2008; 132:983–995. [PubMed: 18358811]

Haarhuis JHI, Elbatsh AMO, Rowland BD. Cohesin and Its Regulation:On the Logic of X-Shaped Chromosomes. Developmental Cell. 2014; 31:7–18. [PubMed: 25313959]

Haering CH, Farcas A-M, Arumugam P, Metson J, Nasmyth K. The cohesin ring concatenates sister DNA molecules. Nature. 2008; 454:297–301. [PubMed: 18596691]

Horsfield JA, Print CG, Mönnich M. Diverse developmental disorders from the one ring: distinct molecular pathways underlie the cohesinopathies. Front Genet. 2012; 3:171. [PubMed: 22988450]

Huang CE, Milutinovich M, Koshland D. Rings, bracelet or snaps: fashionable alternatives for Smc complexes. Philosophical Transactions of the Royal Society B: Biological Sciences. 2005; 360:537–542.

Huis in 't Veld PJ, Herzog F, Ladurner R, Davidson IF, Piric S, Kreidl E, Bhaskara V, Aebersold R, Peters JM. Characterization of a DNA exit gate in the human cohesin ring. Science. 2014; 346:968–972. [PubMed: 25414306]

Ivanov D, Nasmyth K. A topological interaction between cohesin rings and a circular minichromosome. Cell. 2005; 122:849–860. [PubMed: 16179255]

Kim H, Loparo JJ. Multistep assembly of DNA condensation clusters by SMC. Nature Communications. 2016; 7:10200.

Kogut I, Wang J, Guacci V, Mistry RK, Megee PC. The Scc2/Scc4 cohesin loader determines the distribution of cohesin on budding yeast chromosomes. Genes Dev. 2009; 23:2345–2357. [PubMed: 19797771]

Kon A, Shih L-Y, Minamino M, Sanada M, Shiraishi Y, Nagata Y, Yoshida K, Okuno Y, Bando M, Nakato R, Ishikawa S, Sato-Otsubo A, Nagae G, Nishimoto A, Haferlach C, Nowak D, Sato Y, Alpermann T, Nagasaki M, Shimamura T, Tanaka H, Chiba K, Yamamoto R, Yamaguchi T, Otsu M, Obara N, Sakata-Yanagimoto M, Nakamaki T, Ishiyama K, Nolte F, Hofmann W-K, Miyawaki S, Chiba S, Mori H, Nakauchi H, Koeffler HP, Aburatani H, Haferlach T, Shirahige K, Miyano S, Ogawa S. Recurrent mutations in multiple components of the cohesin complex in myeloid neoplasms. Nat. Genet. 2013; 45:1232–1237. [PubMed: 23955599]

Krantz ID, McCallum J, DeScipio C, Kaur M, Gillis LA, Yaeger D, Jukofsky L, Wasserman N, Bottani A, Morris CA, Nowaczyk MJM, Toriello H, Bamshad MJ, Carey JC, Rappaport E, Kawauchi S, Lander AD, Calof AL, Li H-H, Devoto M, Jackson LG. Cornelia de Lange syndrome is caused by mutations in NIPBL, the human homolog of Drosophila melanogaster Nipped-B. Nat. Genet. 2004; 36:631–635. [PubMed: 15146186]

Ladurner R, Bhaskara V, Huis In 't Veld PJ, Davidson IF, Kreidl E, Petzold G, Peters J-M. Cohesin's ATPase activity couples cohesin loading onto DNA with Smc3 acetylation. Curr. Biol. 2014; 24:2228–2237. [PubMed: 25220052]

Laloraya S, Guacci V, Koshland D. Chromosomal addresses of the cohesin component Mcd1p. J Cell Biol. 2000; 151:1047–1056. [PubMed: 11086006]

Lee JY, Finkelstein IJ, Arciszewska LK, Sherratt DJ, Greene EC. Single-molecule imaging of FtsK translocation reveals mechanistic features of protein-protein collisions on DNA. Mol. Cell. 2014; 54:832–843. [PubMed: 24768536]

Lengronne A, Katou Y, Mori S, Yokobayashi S, Kelly GP, Itoh T, Watanabe Y, Shirahige K, Uhlmann F. Cohesin relocation from sites of chromosomal loading to places of convergent transcription. Nature. 2004; 430:573–578. [PubMed: 15229615]

Lengronne A, McIntyre J, Katou Y, Kanoh Y, Hopfner K-P, Shirahige K, Uhlmann F. Establishment of sister chromatid cohesion at the S. cerevisiae replication fork. Mol. Cell. 2006; 23:787–799. [PubMed: 16962805]

Lopez-Serra L, Kelly G, Patel H, Stewart A, Uhlmann F. The Scc2-Scc4 complex acts in sister chromatid cohesion and transcriptional regulation by maintaining nucleosome-free regions. Nat. Genet. 2014; 46:1147–1151. [PubMed: 25173104]

Marquis KA, Burton BM, Nollmann M, Ptacin JL, Bustamante C, Ben-Yehuda S, Rudner DZ. SpoIIIE strips proteins off the DNA during chromosome translocation. Genes Dev. 2008; 22:1786–1795. [PubMed: 18593879]

Michaelis C, Ciosk R, Nasmyth K. Cohesins: chromosomal proteins that prevent premature separation of sister chromatids. Cell. 1997; 91:35–45. [PubMed: 9335333]

Mizuguchi T, Fudenberg G, Mehta S, Belton J-M, Taneja N, Folco HD, FitzGerald P, Dekker J, Mirny L, Barrowman J, Grewal SIS. Cohesin-dependent globules and heterochromatin shape 3D genome architecture in S. pombe. Nature. 2014; 516:432–435. [PubMed: 25307058]

Moreno-Herrero F, de Jager M, Dekker NH, Kanaar R, Wyman C, Dekker C. Mesoscale conformational changes in the DNA-repair complex Rad50/Mre11/Nbs1 upon binding DNA. Nature. 2005; 437:440–443. [PubMed: 16163361]

Moyle-Heyrman G, Zaichuk T, Xi L, Zhang Q, Uhlenbeck OC, Holmgren R, Widom J, Wang J-P. Chemical map of Schizosaccharomyces pombe reveals species-specific features in nucleosome positioning. PNAS. 2013; 110:20158–20163. [PubMed: 24277842]

Murayama Y, Uhlmann F. Biochemical reconstitution of topological DNA binding by the cohesin ring. Nature. 2014; 505:367–371. [PubMed: 24291789]

Nasmyth K. Cohesin: a catenase with separate entry and exit gates? Nat Cell Biol. 2011; 13:1170–1177. [PubMed: 21968990]

Nasmyth K, Haering CH. Cohesin: its roles and mechanisms. Annu. Rev. Genet. 2009; 43:525–558. [PubMed: 19886810]

Novikov DS, Fieremans E, Jensen JH, Helpern JA. Random walks with barriers. Nature Physics. 2011; 7:508–514. [PubMed: 21686083]

Ocampo-Hafalla MT, Uhlmann F. Cohesin loading and sliding. Journal of Cell Science. 2011; 124:685–691. [PubMed: 21321326]

Onn I, Koshland D. In vitro assembly of physiological cohesin/DNA complexes. PNAS. 2011; 108:12198–12205. [PubMed: 21670264]

Peters J-M, Tedeschi A, Schmitz J. The cohesin complex and its roles in chromosome biology. Genes Dev. 2008; 22:3089–3114. [PubMed: 19056890]

Roig MB, Löwe J, Chan K-L, Beckouët F, Metson J, Nasmyth K. Structure and function of cohesin's Scc3/SA regulatory subunit. FEBS letters. 2014; 588:3692–3702. [PubMed: 25171859]

Sjögren C, Nasmyth K. Sister chromatid cohesion is required for postreplicative double-strand break repair in Saccharomyces cerevisiae. Curr. Biol. 2001; 11:991–995. [PubMed: 11448778]

Slutsky M, Mirny LA. Kinetics of Protein-DNA Interaction: Facilitated Target Location in Sequence-Dependent Potential. Biophys J. 2004; 87:4021–4035. [PubMed: 15465864]

Soh Y-M, Bürmann F, Shin H-C, Oda T, Jin KS, Toseland CP, Kim C, Lee H, Kim SJ, Kong M-S, Durand-Diebold M-L, Kim Y-G, Kim HM, Lee NK, Sato M, Oh B-H, Gruber S. Molecular basis for SMC rod formation and its dissolution upon DNA binding. Mol. Cell. 2015; 57:290–303. [PubMed: 25557547]

Song J, Lafont A, Chen J, Wu FM, Shirahige K, Rankin S. Cohesin acetylation promotes sister chromatid cohesion only in association with the replication machinery. J Biol Chem. 2012; 287:34325–34336. [PubMed: 22896698]

Wendt KS, Yoshida K, Itoh T, Bando M, Koch B, Schirghuber E, Tsutsumi S, Nagae G, Ishihara K, Mishiro T, Yahata K, Imamoto F, Aburatani H, Nakao M, Imamoto N, Maeshima K, Shirahige K, Peters J-M. Cohesin mediates transcriptional insulation by CCCTC-binding factor. Nature. 2008; 451:796–801. [PubMed: 18235444]

Williams RS, Moncalian G, Williams JS, Yamada Y, Limbo O, Shin DS, Groocock LM, Cahill D, Hitomi C, Guenther G, Moiani D, Carney JP, Russell P, Tainer JA. Mre11 dimers coordinate DNA end bridging and nuclease processing in double-strand-break repair. Cell. 2008; 135:97–109. [PubMed: 18854158]

Zabrady K, Adamus M, Vondrova L, Liao C, Skoupilova H, Novakova M, Jurcisinova L, Alt A, Oliver AW, Lehmann AR, Palecek JJ. Chromatin association of the SMC5/6 complex is dependent on binding of its NSE3 subunit to DNA. Nucleic Acids Research. 2016; 44:1064–1079. [PubMed: 26446992]

Zhang N, Kuznetsov SG, Sharan SK, Li K, Rao PH, Pati D. A handcuff model for the cohesin complex. J Cell Biol. 2008; 183:1019–1031. [PubMed: 19075111]
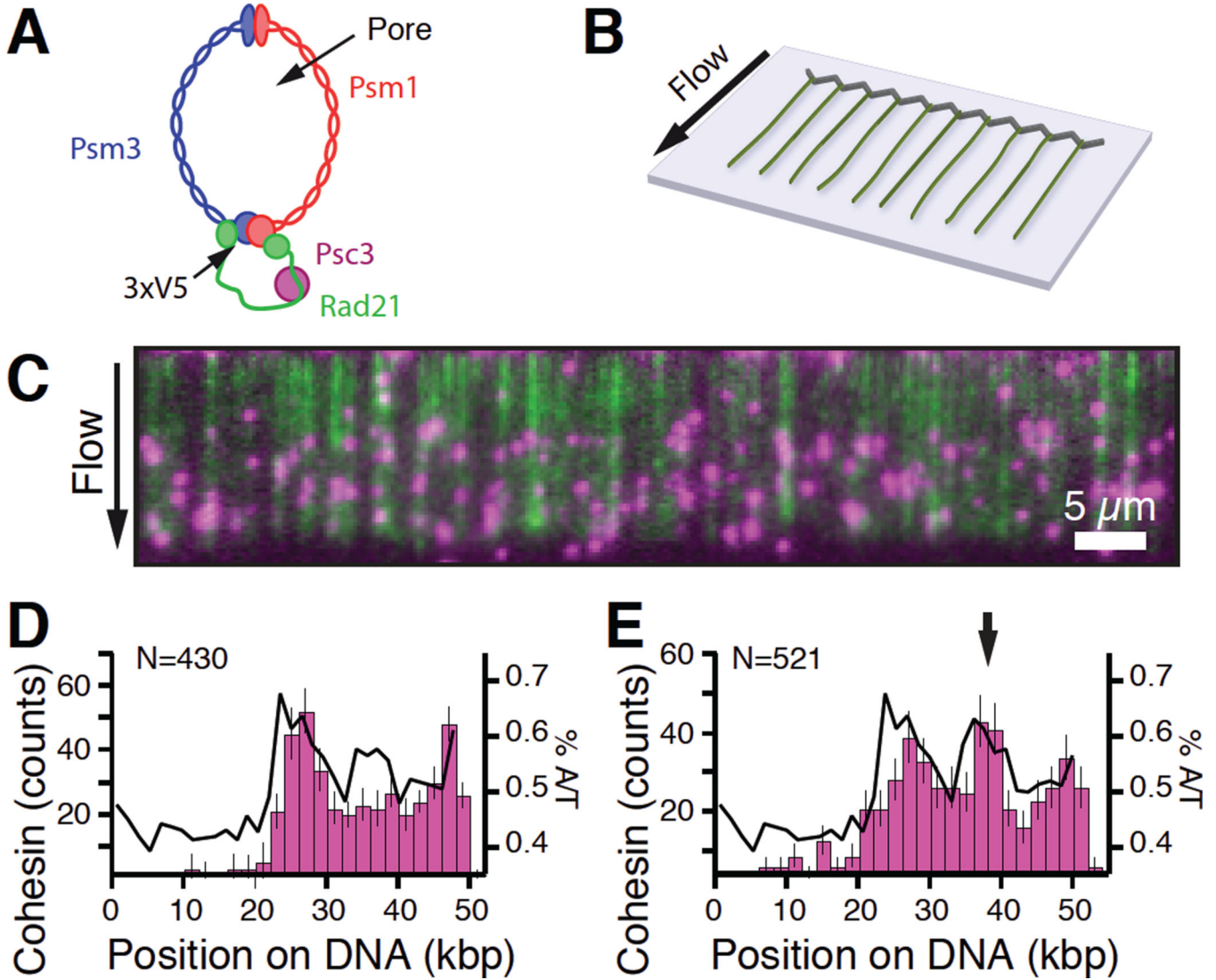
Figure 1.
Single-tethered DNA curtain assays for visualizing cohesin. (**A**) Illustration of cohesin. (**B**) Schematic of a single-tethered DNA curtain. (**C**) Image of a single-tethered DNA curtain bound by cohesin. DNA molecules are in green and cohesin is in magenta. (**D**) Binding distribution of cohesin on λ-DNA (λ^{wt}). The black line illustrates the %A/T content. (**E**) Binding distribution of cohesin on λ-DNA harboring a 3-kb CAR insert (λ^{CAR}). The arrowhead highlights the new peak of cohesin binding, which is attributed to association with CAR. Also see Figure S2A.
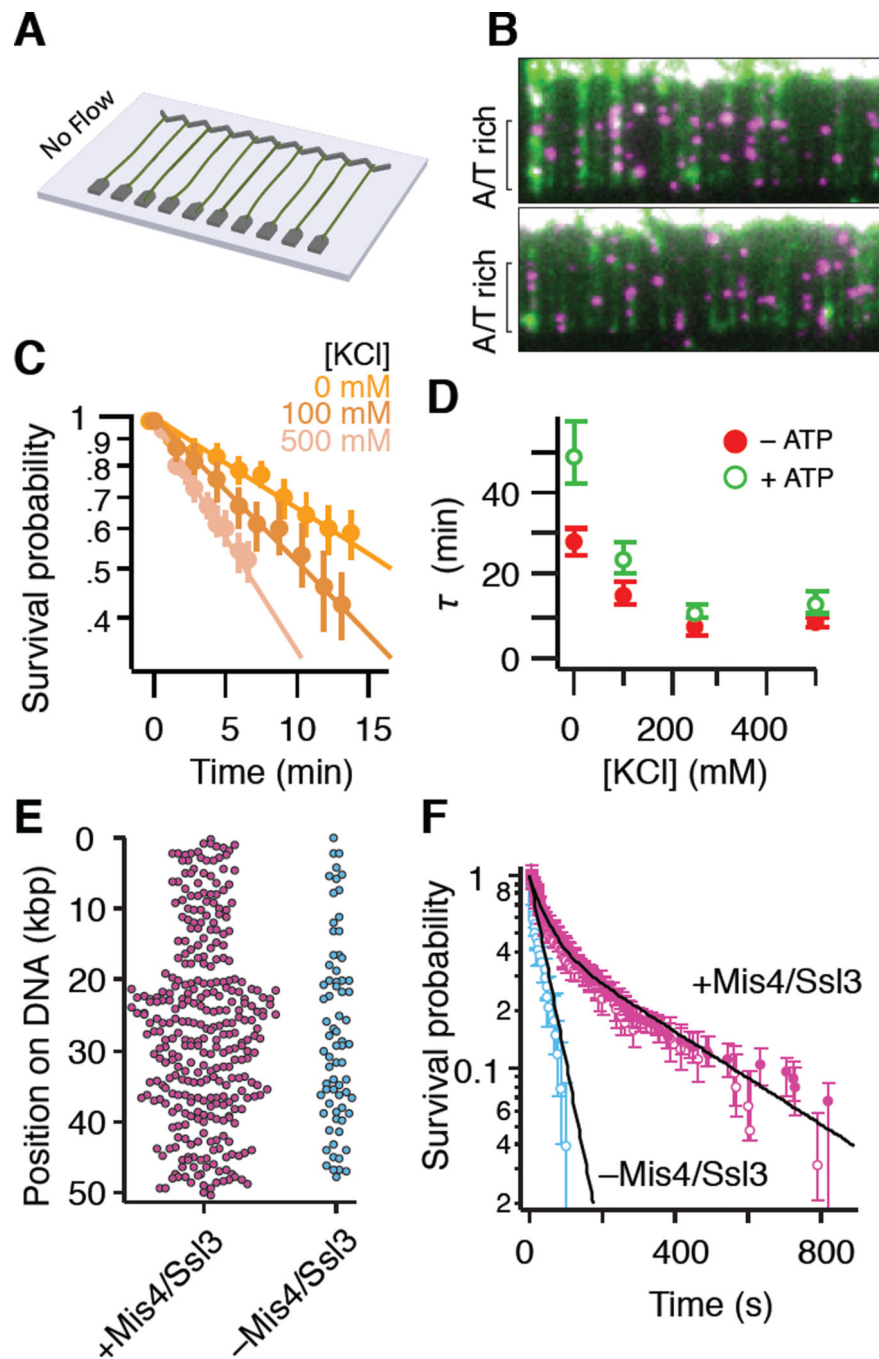
Figure 2.
Double tethered DNA curtain assays for visualizing cohesin in the absence of flow. (**A**)
Schematic of a double-tethered DNA curtain. (**B**) Images of QD-tagged cohesin (magenta)
bound to YOYO1-stained DNA (green). (**C**), Survival probability plots of cohesin at
different KCl concentrations. (**D**) Lifetimes of cohesin on DNA at various concentrations of
KCl in the absence or presence of ATP. (**E**) Initial binding positions of cohesin on λ^{CAR}
±Mis4/Ssl3. (**F**) Transient binding lifetimes of cohesin on λ^{CAR} ±Mis4/Ssl3. Only
complexes that dissociated during the time of the experiment (non-topologically loaded

complexes) were counted. Empty circles: −ATP, filled circles: +ATP. Continuous lines are fits to a single exponential (−Mis4/Ssl3) or double exponential (+Mis4/Ssl3). Error bars are 68% confidence intervals.
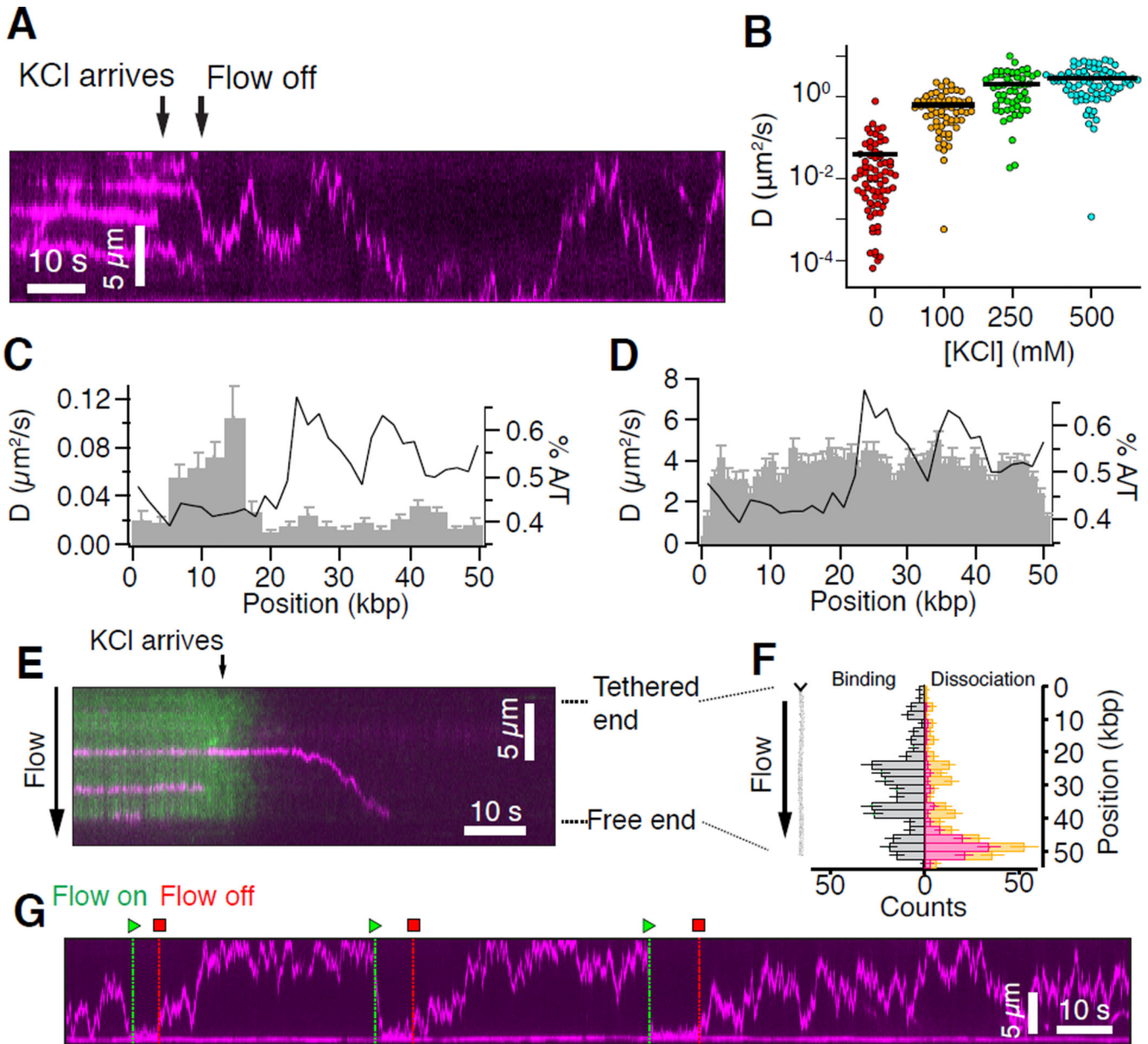
Figure 3.
Cohesin undergoes rapid 1D diffusion. (**A**) Kymograph showing cohesin bound at 0-mM KCl and then chased with 500-mM KCl. (**B**) Cohesin diffusion coefficients as a function of ionic concentration. (**C**) Cohesin diffusion coefficients at different regions of λ^{CAR} at 0-mM KCl and (**D**) 500-mM KCl (see supplemental methods). (**E**) End-dependent cohesin dissociation from a single-tethered DNA when chased with 250-mM KCl; note that YOYO1 is displaced at high salt. (**F**) Cohesin binding distributions prior to KCl arrival (grey bars), and the locations from which cohesin dissociated when chased with high KCl; orange bars include the total population, including proteins that immediately dissociated, red bars correspond to the dissociation positions of proteins that are pushed along the DNA. Also see

Figure S2B. (**G**) Kymograph showing cohesin on a double-tethered DNA in 500-mM KCl during reiterative pulses of buffer flow. Error bars are 68% confidence intervals.
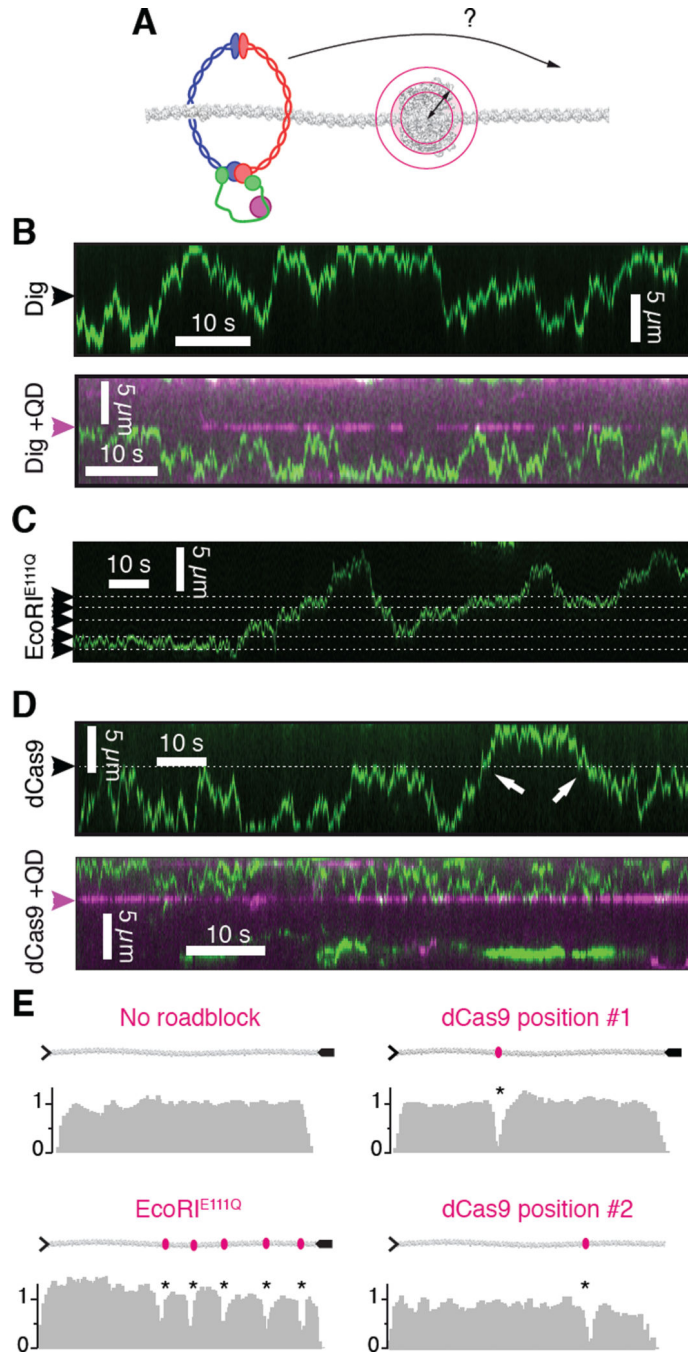
Figure 4.
Obstacles restrict the movement of cohesin. (**A**) Experimental design; concentric red circles depict obstacles of varying diameters (see Figure S3D, S5). (**B**) Kymographs showing cohesin (green) diffusion along DNA (unlabeled) covalently tagged with digoxigenin (Dig) and digoxigenin coupled to a QD (magenta). (**C**) Cohesin diffusing on DNA bound by EcoRI[E111Q]; the locations of the five EcoRI sites are highlighted. Also see Figure S6A. (**D**) Kymographs showing cohesin (green) diffusion along DNA (unlabeled) bound by unlabeled dCas9 or dCas9 labelled with a QD (magenta). Also see Figure S6B. (**E**) Permeability index

plots for cohesin on naked DNA, DNA bound by unlabeled EcoRI[E111Q], and DNA bound by unlabeled dCas9 targeted to two different locations. Illustrations depict DNA orientation, and magenta dots show the locations of the EcoRI[E111Q] and dCas9. The black bar corresponds to $\mu=1$.
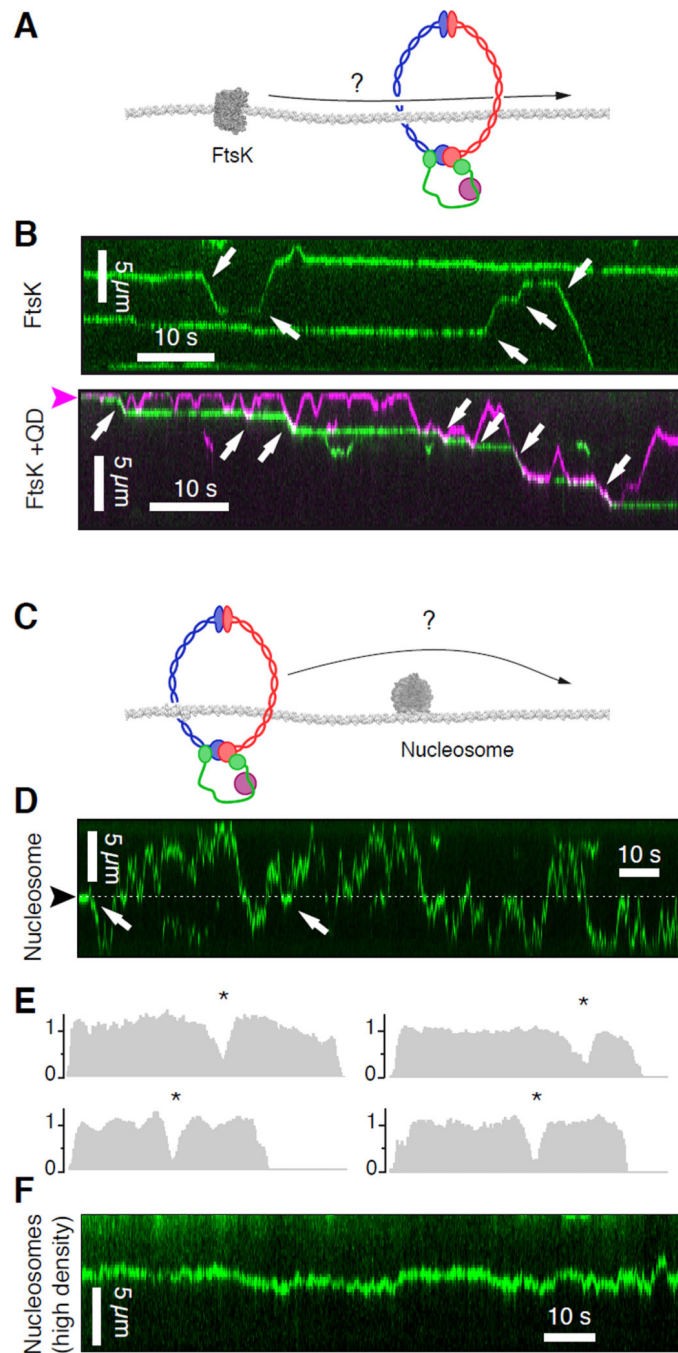
Figure 5.
Influence of nucleosomes and motor proteins on cohesin. (**A**) Experimental design to test whether FtsK can pass through or push cohesin. (**B**) Kymographs showing that FtsK (±QD; magenta) can push cohesin (green) along DNA. Arrows indicate pushes. (**C**) Experimental design to determine whether cohesin can bypass nucleosomes. (**D**) Kymograph showing cohesin on DNA bound by single (unlabeled) nucleosomes. The position of the nucleosome, is indicated. Arrows indicate transient pauses at the nucleosome. Also see Figure S6C. (**E**) Permeability index for cohesin on DNA bound by single nucleosomes; asterisks show the

locations of the nucleosomes. The black bar corresponds to μ=1. (**F**) Kymograph showing diffusion of cohesin along DNA occupied by ~10–50 nucleosomes.
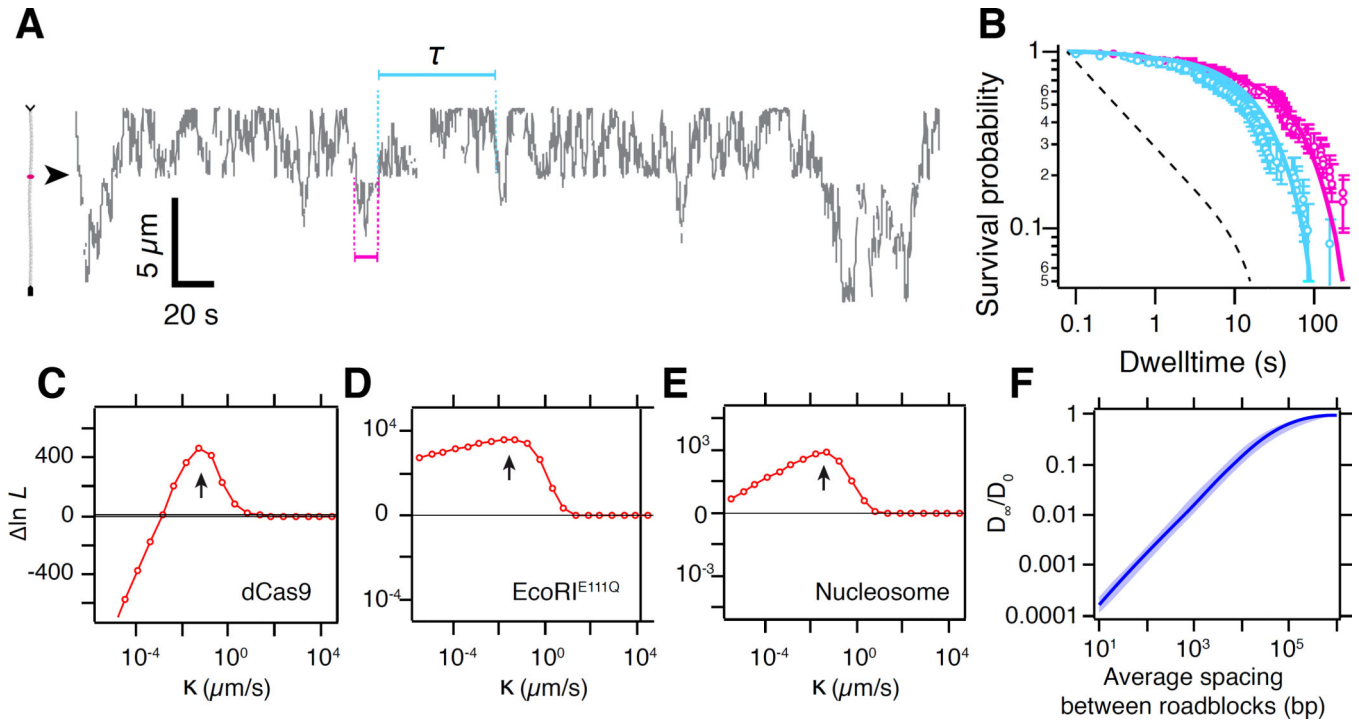
Figure 6.
Extraction of microscopic obstacle permeabilities from diffusion trajectories of single cohesin complexes on obstacle-bound DNA. (**A**) Trajectory of cohesin diffusing on DNA with a dCas9 roadblock bound at the indicated position (arrow). We collect the dwell times of cohesin in the domain on top (cyan) and below (magenta) the obstacle. (**B**) Survival plot of the determined dwell times with fits to a diffusive bypass model (see supplemental methods). The dashed line shows the expected outcome for no roadblock ($\kappa = \infty$), corresponding to frequent crossings of the indicated position. (**C–E**) Log-likelihood $\Delta \ln L = \ln L(\kappa) - \ln L(\infty)$ as a function of the permeability κ for single obstacles of dCas9, EcoRI^{E111Q} and nucleosome. Peaks (arrows) determine the likeliest value of κ (72±10-nm/s for dCas9; 36±7-nm/s for EcoRI^{E111Q}; 38±14-nm/s for nucleosomes). (**F**) Ratio of the effective diffusion coefficient to the free diffusion coefficient D_∞/D_0 on DNA covered with obstacles (of the size of a nucleosome) as a function of spacing between the obstacles. Shaded area: 68% prediction interval.
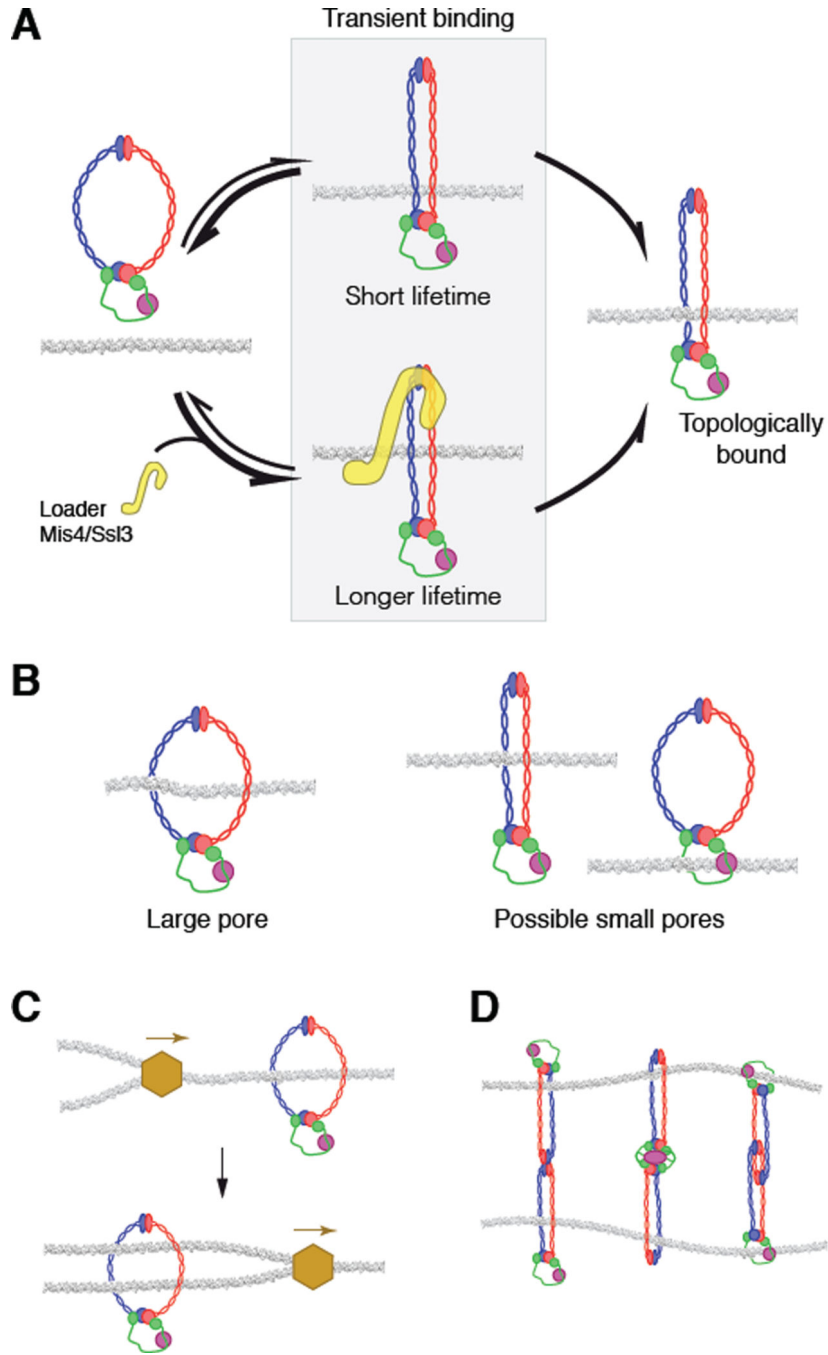
Figure 7.
(**A**) Model for cohesin loading. Cohesin alone shows only short transient binding events with DNA. Mis4/Ssl3 increases both the lifetime and number of these initial binding events, thus promoting the intrinsic ability of cohesin to topologically load onto DNA. (**B**) Illustrations showing the small and large pore models for cohesin. (**C**) Model for sister chromatid cohesion establishment by passage of the replisome through the cohesin ring

(Lengronne et al., 2006). (**D**) Models for sister chromatid cohesion by dimeric rings that do not require a large central pore (Huang et al., 2005; Zhang et al., 2008).